UNIVERSITY OF LEEDS

This is a repository copy of *Modelling the morphology of crystalline deposits evolving from impinging droplets of salt solution*.

White Rose Research Online URL for this paper:
https://eprints.whiterose.ac.uk/78806/

Version: Accepted Version

Proceedings Paper:
Dawson, M, Borman, DJ, Hammond, R et al. (2 more authors) (2014) Modelling the morphology of crystalline deposits evolving from impinging droplets of salt solution. In: Proceedings of the 9th South African Conference on Computational and Applied Mechanics. 9th South African Conference on Computational and Applied Mechanics, 14-16 Jan 2014, Somerset West. . ISBN 978-0-620-58994-9

Reuse
Items deposited in White Rose Research Online are protected by copyright, with all rights reserved unless indicated otherwise. They may be downloaded and/or printed for private study, or other acts as permitted by national copyright laws. The publisher or other rights holders may allow further reproduction and re-use of the full text version. This is indicated by the licence information on the White Rose Research Online record for the item.

Takedown
If you consider content in White Rose Research Online to be in breach of UK law, please notify us by emailing eprints@whiterose.ac.uk including the URL of the record and the reason for the withdrawal request.

White Rose university consortium
Universities of Leeds, Sheffield & York

eprints@whiterose.ac.uk
https://eprints.whiterose.ac.uk/

9th South African Conference on Computational and Applied Mechanics
Somerset West
14 – 16 January 2014

Modelling the morphology of crystalline deposits evolving from impinging droplets of salt solution

Michael Dawson*[I], Duncan Borman[II], Robert Hammond[I], Daniel Lesnic[III], Dominic Rhodes[IV].

[I] School of Process, Environmental and Materials Engineering, [II] School of Civil Engineering, [III] School of Mathematics, University of Leeds, Woodhouse Lane, LS2 9JT, Leeds, UK.

[IV] National Nuclear Laboratory, Sellafield, Seascale, Cumbria, CA20 1PG, UK

Corresponding email:pm09mcd@leeds.ac.uk

Abstract: The work here develops a new moving boundary model which adapts and advances a technique initially used for the purpose of modelling geological formations to predict the morphology of crystallising droplets of salt solution. A multiphase Volume of Fluid (VOF) CFD model coupled with a scalar advection-diffusion transport equation is used to capture the flow and concentration of the solution. By utilising user-defined routines, we are able to couple the models for the solution flow with a crystal growth model. This coupled model captures the growth of the overall bulk crystalline formation by the use of moving boundary techniques with dynamic remeshing of the numerical grid. In this paper an axisymmetric representation of the model is presented that describes the crystal growth through time. The model is compared against data from an experimental study using a simulant salt solution (Sodium Nitrate) where physical parameters and growth rates predicted by the model are in good agreement with those observed in experiments. These studies provide information for the safety assessment when considering heavy metal solutions for various fault scenarios.

Keywords: Computational Fluid Dynamics, Mass Transfer, Moving Boundary Problem, Nuclear Safety.

1 INTRODUCTION

Crystallisation is the key underlying physical process in a wide range of industries. Computational or numerical models that describe crystallisation processes can offer a range of industrial benefits, such as developing an understanding of how particular parameters or process equipment can influence crystal growth, hence allowing manufacturers to optimise the yield and quality of produced crystals. It is therefore no surprise that the demand for models that can accurately describe the crystallisation process is very high. An example of an industry where computational models are used in order to analyse and optimise the manufacture process is the sugar industry, as seen in Sima and Harris [1]. Another industry where models are beneficial is the pharmaceutical industry, where they can provide an understanding of how process parameters affect the final morphology of the crystal, an example of which can be seen in Chen et al [2]. Understanding of the crystallisation process is also of key importance in industries that are not primarily concerned with the production of crystalline materials, but where crystals are the undesirable by-product of an unrelated or adverse occurrence. Examples of these include pipe or heat exchanger fouling, as in Choi et al [3], or the build-up of unwanted deposits from a pipe or vessel leakage. The ability to model and describe the formation of crystalline deposits arising from adverse occurrences is of particular importance within the

nuclear industry. It is known that for a given formation, its size and shape impacts on the criticality risk, as explained in Knief [4]. Therefore models which can predict these formations, using known process parameters, can aid in the costing and risk assessment of clean up procedures.

In light of this, several experiments have previously been carried out by the National Nuclear Laboratory (NNL), using stimulant solutions of Sodium Nitrate, in order to assess how varying chemical and environmental parameters affect the resultant build up of material. The experimental results demonstrate that a diverse range of crystalline formations can occur for varying experiment parameters; tower type formations for saturated solutions ($\geq$8 Molar at 30°C), as shown in Figure 1a, and ring-like formations for under-saturate solutions ($\leq$5 Molar in this case), as shown in Figure 1b. Clearly, the criticality implications of these formations change quite drastically for small changes in the experimental parameters.

The work in this paper attempts to model the crystallisation of impinging droplets of salt solution. The aim of this work is to offer insight into the size and shape of crystalline deposits which may occur from droplets of industrial process liquor, arising from a long term undetected equipment or pipe leakage. The modelling here will be restricted to the case of saturate solutions only.

Previous work adapted models for describing the growth of geological stalagmites, seen in Romanov et al [5], for the purpose of modelling crystallisation of salt solution droplets. This work was based on simple analytical expressions for the fluid flow. Despite this, results from this study were promising. Work here now advances these models using computational fluid dynamics (CFD) and advanced physical models.

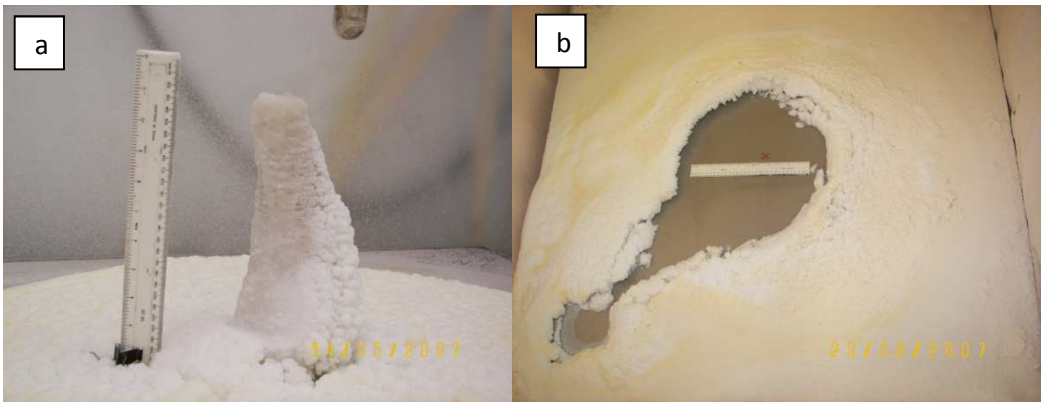

Figure 1 Image of crystalline growth after 30 days for a) highly concentrated Sodium Nitrate droplets and b) undersaturate droplets.

2 MATHEMATICAL MODEL

In this work we assume that droplets impact on the surface of an inclined plate. After impact, droplets coalesce to form a thin liquid film, which in turn, flows down the incline of the plate. Due to temperature loss and evaporation, solubility within the film decreases and crystallisation occurs. The continually fed liquid film then adapts to flow over the newly formed crystalline solids.

2.1 Fluid and Mass Transport

A numerical scheme is needed in order to capture the thin liquid film as it flows down the inclined plate. There are currently many numerical models designed for capturing the flow of multiple fluids. Here we use the volume of fluid (VOF) method which is specifically designed for the modelling of immiscible fluids and capturing the interface between the two. The modelling of film flow is a common problem, as it is a phenomenon which occurs in many industrial processes. It is common practice when modelling these flows

to use the VOF method, as seen in Haroun et al [6] and Hirt and Nichols [7]. It is particularly important that the flow and interface are captured accurately as the velocity and thickness of the liquid film is likely to have a direct impact on the rate of crystallisation.

As the crystal growth is a much slower physical process than that of the fluid flow we assume that within a specified time frame, Δt (the pseudo-timestep), the crystal can be assumed stationary and the fluid flow can be approximated by a steady state solution. As the total timeframe for crystal growth in these problems tends to span weeks or even months, obtaining a fully transient CFD simulation over these timeframes would generally be consider infeasible. Due to this assumption we track the interface between the liquor solute and gaseous phase by solution of the volume fraction equation, given by,

$$\nabla \cdot \left(\alpha_q \rho_q \mathbf{u}\right) = S_{\alpha_q}, \quad 0 \leq \alpha_q \leq 1, \quad \text{for } q = 2, .., n, \tag{1}$$

where ρ_q is the density of the qth phase, S_{α_q} is a the source term relating to the qth phase, α_q is the volume fraction with respect to the qth phase, n represents the number of phases and $\mathbf{u}$ is the veolcity. The volume fraction equation is not solved for $q = 1$ and is calculated by the fact that in each computational cell,

$$\sum_{q=1}^{n} \alpha_q = 1, \tag{2}$$

The fluid velocity, $\mathbf{u}$, is obtained using a single equation approach, where both the transport of momentum within the liquid and gases phase can be described by the Navier-Stokes equations,

$$\frac{1}{\rho}\nabla p + (\mathbf{u} \cdot \nabla)\mathbf{u} = \nu \nabla^2 \mathbf{u} + \mathbf{g}, \qquad \nabla \cdot \mathbf{u} = \mathbf{0}, \tag{3}$$

where ρ is the fluid density, p is the pressure, $\mathbf{g}$ is the acceleration due to gravity oriented parallel to the y-axis in Figure 2, μ is the dynamic viscosity and $\nu = \frac{\mu}{\rho}$ is the kinematic viscosity. This shared field approach is dependent on the volume fractions of the phases though the properties of ρ and μ, where,

$$\rho = \sum_{q=1}^{n} \alpha_q \rho_q, \tag{4}$$

such that ρ_q is the fluid density with respect to the qth phase and,

$$\mu = \sum_{q=1}^{n} \alpha_q \mu_q, \tag{5}$$

where μ_q is the dynamic viscosity with respect to the qth phase.

Transportation of solute within the solution is described by solution of a scalar advection-diffusion equation. At steady state and when coupled to the VOF method, this equation is given by,

$$\mathbf{u} \cdot \nabla(\alpha_2 c) = \nabla \cdot (\alpha_2 D \nabla c), \tag{6}$$

where c is the concentration of Sodium Nitrate in solution and D is the diffusion coefficient. In this work, $q = 1$ corresponds to the gaseous phase, air, and $q = 2$ corresponds to the liquid solution consequently, α_2 is the volume fraction of the liquid phase.

The viscosity and density of the solution is dependant on the local concentration of solute such that, $\rho_2 = f(c)$ and $\mu_2 = g(c)$, where f and g are dependent on the material in question, and will be defined in section 3.

2.2 Solvent Evaporation

In many physical processes evaporation is the dominant driving force for crystallisation. This is true for the NNL drip trials and therefore a numerical method of capturing the evaporation phenomenon was

considered. Evaporative effects are often included within CFD models that predominantly look at either the evaporation of liquid films, observed in Avc et al [8], or the evaporation of sessile droplets, shown in Sazhin [9]. Applications for such models are extensive ranging from, the drying of paper within the textile industry to the de-icing of aircraft systems.

In this work, a constant evaporative flux will be considered, where flux values will be based around measurements from the NNL drip trials. Only the loss of mass from the liquid phase will be considered, and therefore the increase in mass due to water vapour will be ignored, $S_{\alpha_1} = 0$ was not invluded in (1).

The source term in (1) is a volumetric flux, whilst evaporation is a surface reaction, therefore the source term must be expressed such that the amount of water extracted is not dependant on the volume of the cells located at the interface. When considering an evaporative flux, E over a surface area A_f, we can state the the rate of mass leaving the volume containing a surface must equal,

$$S_{\alpha_2} V_{cell} = -E A_f, \tag{7}$$

where V_{cell} is the volume of the cell, $E > 0$ is the evaporative flux, and A_f is the interfacial area of the free surface contained within the cell. Clearly, this allows one to express the volumetric source, S_{α_2} in terms of the current cell volume and interfacial area, to ensure the correct rate of liquid is extracted from the system.

As the VOF model is a diffusive numerical scheme, the lack of a well defined interface can make it difficult to give a value for the interfacial area, A_f. Within this work we employ a technique used within Hardt and Wondra [10], which incorporates an evaporative model for use with the VOF model. This states that

$$\int_\Omega |\nabla \alpha_2| d\Omega = \int_A dA, \tag{8}$$

where Ω is a volume containing the liquid-gas interface, $|\nabla \alpha_2|$ is the magnitude of the gradient vector of the volume fraction of water, and A is the interfacial surface area within the volume Ω. Therefore for an individual cell, the following holds,

$$|\nabla \alpha_2| V_{cell} = A_f, \tag{9}$$

which allows the source term in (7) to be written as,

$$S_{\alpha_2} = -E |\nabla \alpha_2|. \tag{10}$$

This term is then included in (1), which accounts for the loss of mass due to evaporation.

2.3 Crystal Growth and Moving Boundary Techniques

The work here is based around two-step crystallisation theories, as seen in Mullin [11]. This model assumes that crystallisation is based around two physical processes, a diffusive step, where solute must diffuse across a mass transfer boundary layer adjecent to the crystal face. Followed by a surface integration step, where after transport across boundary layer, solute is incorporated into the crystalline lattice. Within this work the transport of solute is captured fully by (6), including the movement of solute through the boundary layer. The surface integration step is incorperated into the model through appropriate boundary conditions. The distance from the crystal surface at which the surface integration step occurs, is generally very small and therefore can be taken to occur on the boundary describing the surface of the crystal. Due to this, we can now describe the flux of solute out of solution at the crystal surface by the boundary condition,

$$-D \frac{\partial c}{\partial \mathbf{n}} = k_r (c - c*), \text{ on the solid-liquid interface,} \tag{11}$$

where $\mathbf{n}$ is the outward unit normal to the boundary, c* is the Sodium Nitrate concentration at equilbrium and $\mathrm{k_r}$ is the rate of surface integration.

Other works have performed similar calculations using momentum and mass transport equations when considering a single phase flow, such as, Robey and Maynes [12] and Robey [13]. These works only observe the concentration field at a fixed snapshot in time. The work here attempts to capture the growth of crystalline material through time by the use of a moving boundary technique coupled to a multiphase fluid model. This will describe how the fluid and mass fields change when coupled to a growing crystalline structure, and simultaneously, how the crystal growth process is affected by the changing flow and solute fields.

The moving boundary technique which is used in order to describe the crystal growth will be described in detail later, however it should be noted that the crystal growth is related to (11) such that,

$$\frac{\partial \mathrm{m}}{\partial \mathrm{t}} = \mathrm{k_r}\frac{\mathrm{M_s}}{\rho_\mathrm{s}}(\mathrm{c} - \mathrm{c}*), \text{ on the solid-liquid interface,} \tag{12}$$

where m is the mass deposited, $\mathrm{M_s}$ is the molar mass of Sodium Nitrate and ρ_s is the density of solid Sodium Nitrate.

3 COMPUTATIONAL IMPLEMENTATION

The model described in section 2 was implemented and solved using the finite volume package Fluent 14.5. The problem was initially solved in two-dimensions in order to assess the accuracy and robustness of the model. It was then later developed into an axisymmetric model, such that the formations could be approximated by a formation with rotational symmetry about the drip location. In this pape,r the computational implementation for the axisymmetrix model will be discussed.

3.1 Moving Boundary and Dynamic Meshing

The computational domain consists of the initial slightly inclined plate at an angle of 2° with the horizontal and a small region above it. Figure 2 demonstrates a typical initial domain used within this problem.

The mass of solute is deposited at the rate given by (12). This deposited mass is represented by the moving boundary model by discrete displacements of the nodes along the floor surface. Nodes are displaced along the normal direction through,

$$(\Delta \mathrm{S})\mathbf{n} = -(\Delta \mathrm{t})\mathrm{k_r}\frac{\mathrm{M_s}}{\rho_\mathrm{s}}(\mathrm{c} - \mathrm{c}*)\mathbf{n}, \text{ on the solid-liquid interface,} \tag{13}$$

where $\Delta \mathrm{t}$ is the 'pseudo time-step', and $\Delta \mathrm{S}$ is the magnitude of the displacement of the boundary in time $\Delta \mathrm{t}$. The crystal or solid-liquid interface is denoted by boundary 'Floor / Crystal Surface' in Figure 2. This displacement is imposed through the use of user defined code. A typical example of the domain after successive boundary displacements can be seen in Figure 3.

After the boundary nodes relating to the crystal interface have been displaced by $\Delta \mathrm{S}$ given in (13), the dynamic meshing routine adjusts the remaining boundaries within the domain such that there remains a small region captured above the crystalline material and the inlet and outlets remain at the appropriate positions throughout the computational procedure. Once these boundaries have moved the dynamic meshing routine updates the computational grid to fit the new boundary positions. The dynamic meshing facility has inbuilt remeshing, where if a given cell either exceeds a maximum volume or is less than a minimum volume or becomes too distorted, the model will attempt to remesh the region local to this cell.

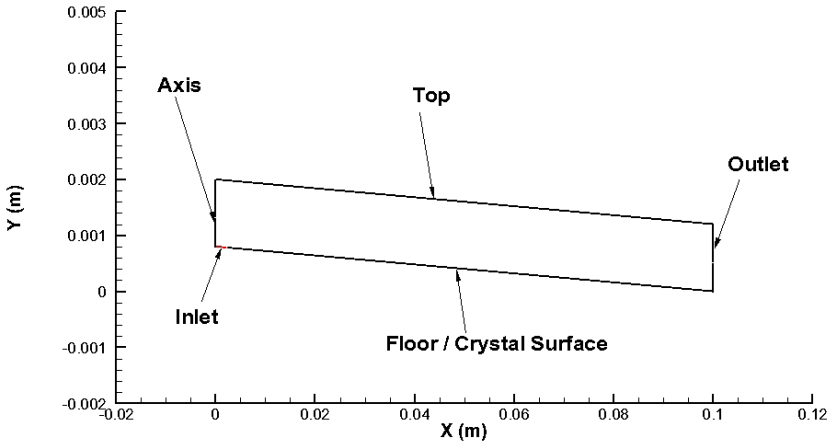

Figure 2 Plot of a typical initial domain, with boundary names.

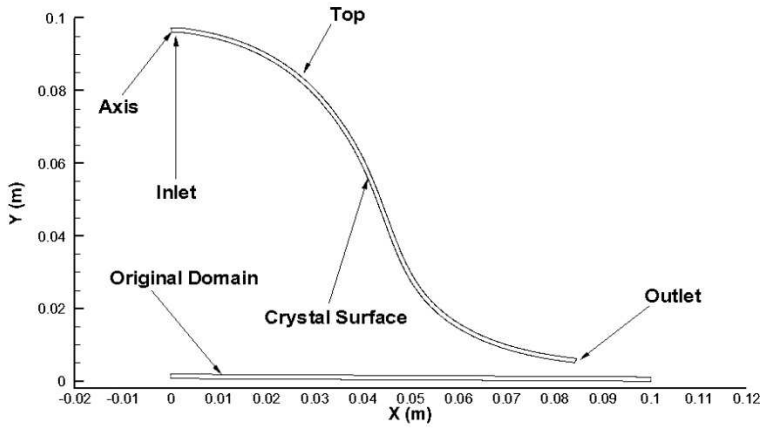

Figure 3 Typical example of the domain after successive boundary motions.

3.2 Computational Grid

The multiphase VOF model being used to capture the fluid flow is a diffusive interface model and therefore, there exists a numerical blending between the two regions. Due to this, a refined region of highly refined region of quadrilateral cells is required within the region of the interface. This is in order to minimise the diffusive flux across the interface. This can be observed within Figure 4.

For dynamic remeshing to work, as mentioned in section 3.1, the mesh must consist of triangular elements (in two dimensions). And therefore the bulk of the computational grid is meshed using these elements, in order that the dynamic remeshing facility remains robust and the computational grid remains of a good quality throughout its continual deformation.

The standard starting mesh for the axisymmetric problem is 91640 cells. Whilst this appears relatively small, studies regarding mesh independence have shown larger mesh sizes have no impact on the final solution.

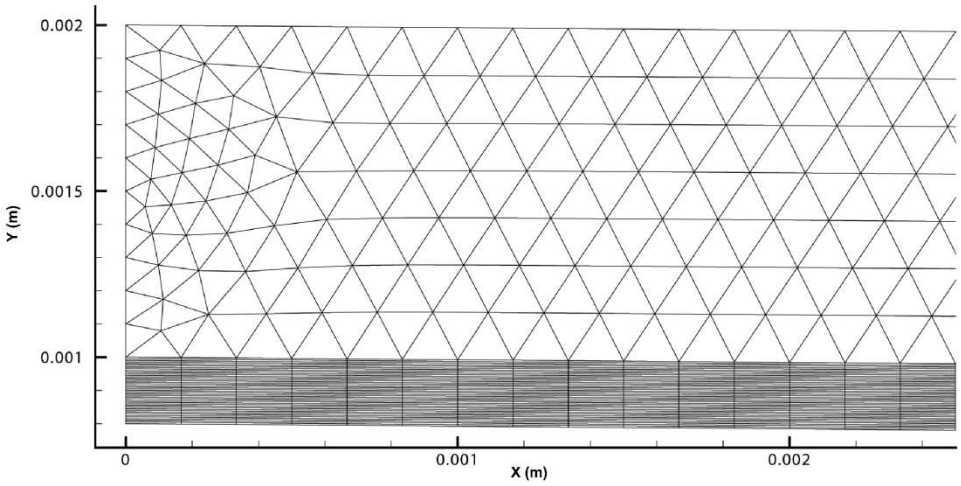

Figure 4 Example of the initial mesh.

3.3 Boundary Conditions

Appropriate boundary conditions must be set for the fluid flow, solute transport and moving mesh equations. An inlet condition joins onto the floor surface and is specified to be roughly the diameter of a liquid droplet. Here a constant mass flow is imposed such that $\mathbf{u} \cdot \mathbf{n}_{\text{inlet}} = \text{Q}/\text{A}$, where Q is the mass flow rate, $\mathbf{u}$ is the velocity, A is the area of the inlet and $\mathbf{n}_{\text{inlet}}$ is the unit vector normal to the inlet. A no-slip boundary condition, such that, $\mathbf{u} = \mathbf{0}$, is imposed on the floor / crystal surface. The outlet and top of the domain are pressure outlets, where a gauge pressure, $\text{p}' = \text{p} - \text{p}_{\text{atm}} = 0$ is specified. Where p is the absolute pressure and p_{atm} is the atmospheric pressure. A constant concentration $\text{c} = \text{c}_0$ is imposed at the inlet and the flux condition (11) on the floor / crystal surface.

3.4 Material Properties

As discussed in section 2, properties within the model are specific to the material in question. These include the density, viscosity, rate of surface integration and the solubility. Within this section these relationships are defined. Custom material properties are implemented through the use of user defined functions in the CFD code. The density of the solution is dependent on both the temperature and the local concentration within the solution. The density and viscosity of Sodium Nitrate solution, in (4), are given by, see Xu and Press [14],

$$\rho_2 = \text{f(c)} = \text{a} - \text{b(T} - 273.15), \ \mu_2 = \text{g(c)} = 10^{-9}\text{A}\sqrt{\text{T}}\text{e}^{\frac{\text{B}}{\text{T}-\text{T}_0}}, \tag{14}$$

where, $\text{a} = 421.37\text{X}^2 + 629.7\text{X} + 1012.6$, $\text{b} = -168.16\text{X}^5 + 206.79\text{X}^4 - 89.845\text{X}^3 + 17.308\text{X}^2 - 0.6854\text{X} + 0.4789$), X is the mass fraction given by, $\text{X} = \frac{\text{c M}_\text{S}}{\text{c M}_\text{S}+1}$, $\text{A} = 4219.6\text{X}^2 + 2995.2\text{X} + 991.72$, $\text{B} = 300834\text{X}^6 + 525458\text{X}^5 - 348368\text{X}^4 + 106051\text{X}^3 + 14531\text{X}^2 - 967.34\text{X} + 644.92$, $\text{T}_0 = 29.088\text{X}^2 + 15.881\text{X} + 134.68$ and T represents the temperature (in K).

In (11) the rate of crystal growth is dependent on the local solubility level, c*, an expression for this when using Sodium Nitrate was obtained empirically in Oosterhof [15], and is given by,

$$\text{c}^* = 8511.90 + 98.45\text{T} \text{ [molar]}, \tag{15}$$

The diffusivity of Sodium Nitrate in solution is set to be a constant value of

$$\text{D} = 1.586 \times 10^{-9} \text{ [m}^2/\text{s]}, \tag{16}$$

which is obtained in Yeh and Wills [16]. This value will vary slightly with temperature and concentration however, in the work here it is assumed constant. The rate of surface integration is

$$\mathrm{k_r} = 4.5\mathrm{e} \times 10^{-6}\ [\mathrm{m/s}], \tag{17}$$

which is also obtained in Oosterhof [15].

We believe that the physical conditions under which equations (14)-(17) were empirically derived in [14]-[16] cover a large enough range, $\mathrm{T} \in (0,40)°\mathrm{C}$ and solution concentrations $\mathrm{c} \in (0,10)\ \mathrm{Molar}$, to include the conditions of our experiment.

Summarising, the solver process initial involves solving equations (1)-(10) for a steady state fluid and solute transport solution using boundary conditions and material properties defined in sections 3.3 and 3.4. The crystal is then grown over a 'pseudo time-step', Δt, using the moving boundary model, given in (13). Once the new boundary position and adjusted domain is obtained, equations (1)-(10) are solved again until convergence is reached, and the process repeats in an iterate manner until the final solution time is obtained.

4 RESULTS

Intially, the model was constructed in two-dimensions such that a robust coupling between the fluid flow model and crystal growth model could be obtained. The work here considers the axisymmetric model where results can now be quantitively compared against physical properties such as experimetal measurement for the size and shape of the formations.

A typical example of results produced by the model can be observed in Figure 5. From Figure 5a one can see how the crystalline material is deposited on the intial flat plate through time. The volume displaced by the boundary represents the growth of crystal. Figure 5a shows that the majority of the solute is deposited close to the drip location.

When considering an axis of rotation at x=0, it is clear to see that the model is predicting tower like formations for the crystallisation of highly concentrated salt solutions, much like the physical case observed in the experiments. From observing Figure 5b it can be confirmed that the full axisymmetric respresentation of the result after 30 days closely resembles the tower-like formations, as seen in Figure 1a. Whilst the idealised mathematical model produces smooth solutions for the crystal surface, unlike the experimental results, the key defining features such as the width and height of the formations are captured well by the model.

Once of the model was shown to be robust, the validity of the model was assessed by comparing it against the experimental data for the Sodium Nitrate drip trials. Within these, trials solutions where brought to saturation at 30℃. This roughly corresponds to an initial concentration, $\mathrm{c_0} = 8$ molar. The solution was then leaked into a room with temperature of approximately T=25℃ at a rate of $\mathrm{Q} = 2.89 \times 10^{-5}$kg/s. The evaporative flux for both the numerical and physical experiments was 1×10^{-5}kg/m^{2}s. In this work, the temerature drop was considered to be instantious and therefore an isothermal system was considered. Non isothermal systems could be considered through solution of the energy equation.

Results for this can be observed in Figure 6. Figure 6a shows a comparison between the experimental data and model results after 30 days growth. From looking at Figure 6a, it can be seen that the profile obtained from the model lies reasonably close to the experimental data. Results close to the apex are slightly smaller than the experimental results, and the width of the tower is slightly thicker in the model.

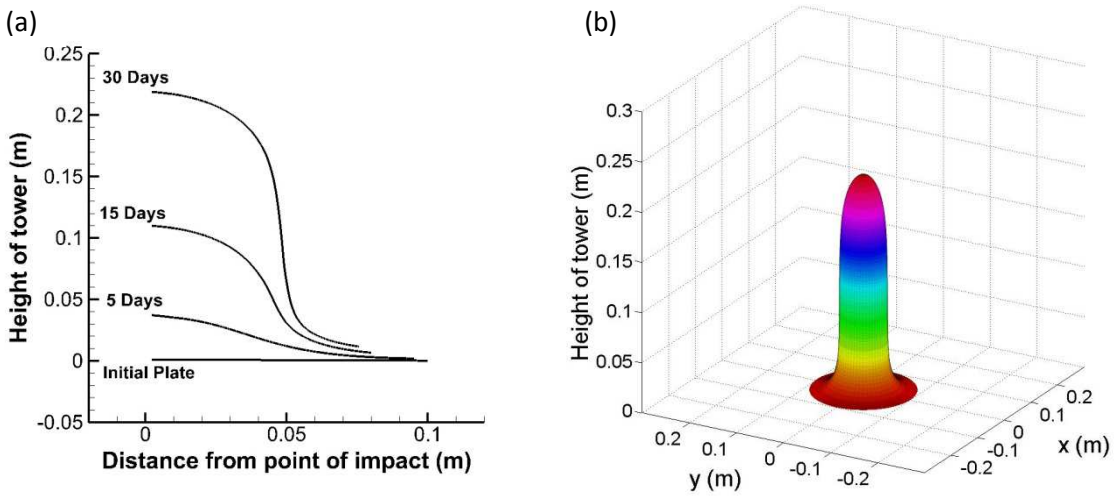

Figure 5 a) Plot of formation profiles through time for the moving boundary model, b) full axisymmetric representation for growth after 30 days.

It is thought that the slight discrepancies in the results may be due to uncertainities (presumed to be of the order 5% noise) in the experimental data. Also, temperature data from the experiments was shown not to be uniformthroughout, but to vary both temporally and spatially, ranging from approximately 22.5℃ to 27.5℃. In order to further assess the model's validity in light of these uncertainities, the model was run again for temperatures of 22.5℃ and 27.5℃. It can be seen from Figure 6a that the experimental data lies within the region between these maximum and minimum temperature variations.

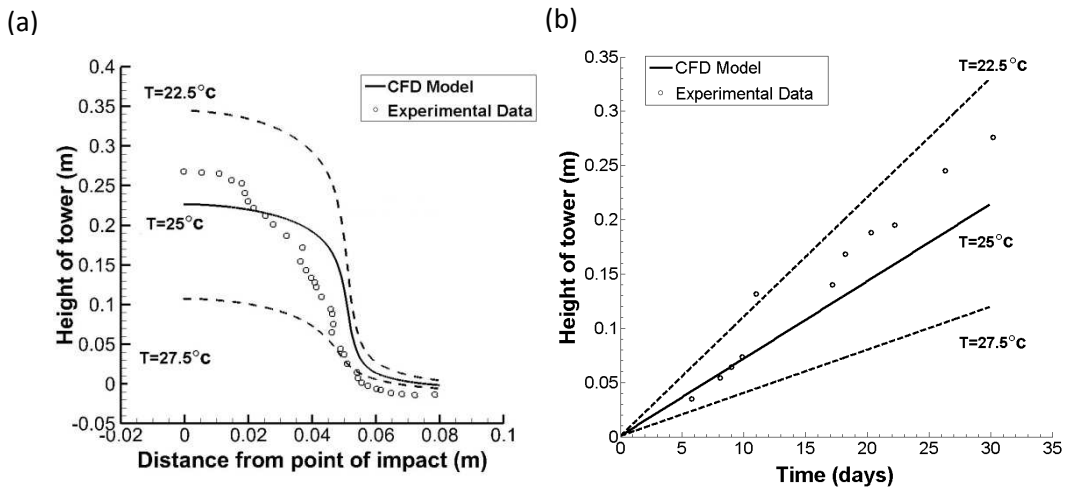

Figure 6 a) Plot of the formation profile for model and experimental data after 30 days growth and b) Plot of the tower height through time.

In addition to the profile of the tower formation plotted after 30 days growth, experimental data for the heights of the tower formations was compared against the model. Figure 6b shows the heights of the tower formations through time when compared to experimental data. From observing Figure 6b it can be seen that the majority of the experimental data points lie within the feasibility region outlined by the solutions at the temperature extremes. At later times, the experimental data tends to lie above the model data for the mean temperature of 25℃.

5 CONCLUSIONS

The first stage of the work was the development and implementation of a two-dimensional model for the purpose of creating a robust framework for coupling the multiphase fluid flow with the moving boundary crystallisation model. The work in this paper now progressed previous work such that an axisymmetric model with rheological, chemical and evaporative effects was developed.

The model was compared against data obtained from experiments carried out by the NNL. Initial results for the model appear promising when compared against the experiments data. Using basic information for the process parameters, material properties and flow conditions the model is able to give a good prediction for both the height and width of the formation. To the authors knowledge no previous models allowed the prediction or estimation of these formation for the aforementioned parameters, therefore it is expected that the work here will have impact on on-going safety cases within the Nuclear Industry.

Additional work may be carried out, including a full parametric study for varying process parameters, in order to generate an accurate risk assessment for likely industrial operating conditions. Further experimental work may be carried out In order to assess the model's validity when used with other materials. Parameters for the use with heavy metal solutions are currently being investigated.

ACKNOWLEDGEMENTS

The authors would like to thank the EPSRC and the NNL for their continual funding and support.

REFERENCES

1 M. Sima and J. Harris. CFD modelling of sucrose crystallisation. Second International Conference on CFD in the Minerals and Process Industries, 1999.

2 J. Chen, B. Sarma, J. M. B. Evans, and A. S. Myerson. Pharmaceutical crystallization. Crystal Growth and Design, 11(4):887–895, 2011.

3 W. Choi, S. Jun, L. Nguyen, N. Rungraeng, H. Yi, S. Balasubramanian, V. Puri, and J. Lee. 3D milk fouling modeling of plate heat exchanges with different surface finishes using computational fluid dynamics codes. Journal of Food Process Engineering, 36: 439–449.2013.

4 R. Knief. Nuclear Criticality Safety: Theory and Practice. American Nuclear Society and U.S. Nuclear Regulatory Commission, 1985.

5 D. Romanov. G Kaufmann, and W. Dreybodt. Modeling stalagmite growth by first principles of chemistry and physics of calcite precipitation. Geochimica et Cosmochimica Acta, 72(2):423-437.

6 Y. Haroun, D. Legendre, and L. Raynal. Volume of fluid method for interfacial reactive mass transfer: Application to stable liquid film. Chemical Engineering Science, 65(10):2896 – 2909, 2010.

7 C. Hirt and B. Nichols. Volume of fluid (VOF) method for the dynamics of free boundaries. Journal of Computational Physics, 39(1):201 – 225, 1981.

8 A. Avc, M. Can, and A. B. Etemolu. A theoretical approach to the drying process of thin film layers. Applied Thermal Engineering, 21(4):465 – 479, 2001.

9 S. Sazhin. Advanced models of fuel droplet heating and evaporation. Progress in Energy and Combustion Science, 32(2):162–214, 2006.

10 S. Hardt and F. Wondra. Evaporation model for interfacial flows based on a continuum-field representation of the source terms. Journal of Computational Physics, 227(11):5871 – 5895, 2008.

11 J.W.Mullin. Crystallization, 4th edition. Butterworth Heinemann, 2001.

12 H. F. Robey and D Maynes. Numerical simulation of the hydrodynamics and mass transfer in the large scale, rapid growth of KDP crystals. Part 1: Computation of the transient, three-dimensional flow field. Journal of Crystal Growth, 222:263-278, 2001.

13 H. F. Robey. Numerical simulation of the hydrodynamics and mass transfer in the large scale, rapid growth of KDP crystals—2: Computation of the mass transfer. Journal of Crystal Growth, 259:388-403, 2003.

14 T. Xu and K. Pruess. Thermophysical properties of sodium nitrate and sodium chloride solutions and their effects on fluid flow in unsaturated media. Technical report, Lawrence Berkeley National Laboratory, 2001.

15 H. Oosterhof. The growth of sodium nitrate from mixtures of water and iso-propoxyethanol. Journal of Crystal Growth, 198:754–759, 1999.

16 H. S. Yeh and G. B. Wills. Diffusion coefficient of sodium nitrate in aqueous solution at 25 deg. as a function of concentration from 0.1 to 1.0M. Journal of Chemical & Engineering Data, 15 (1), 187-189, 1970.